# Modeling of structure and vibrational spectra of aluminophosphate AlPO4 5 and its silica analog SSZ 24

# Modeling of structure and vibrational spectra of $AlPO_4$-5 and its silica analog SSZ-24

**A.J.M. de Man,* W.P.J.H. Jacobs,* J.P. Gilson,† and R.A. van Santen***
**Schuit Institute of Catalysis, Eindhoven University of Technology, Eindhoven, The Netherlands*

*†Koninklijke/Shell Laboratory (Shell Research), Amsterdam, The Netherlands*

In this study, the structural and vibrational properties of the $AlPO_4$ structure $AlPO_4$-5 and the silica structure SSZ-24 are compared. Lattice energy calculations are done using existing potential parameter sets suitable for silicas and $AlPO_4$'s. For the computation of vibrational spectra of silica systems, force constants derived by Etchepare et al. are used. For $AlPO_4$ spectra simulations, a new force field is presented that is based on a fit on vibrational frequencies of α-berlinite, the $AlPO_4$ analog of α-quartz. Lattice energy calculations result in a symmetry of $AlPO_4$-5 and SSZ-24 that is lower than derived experimentally. A shift of layers is observed for both structures when a potential with partial charges is used. This shift is not found for a formally charged shell model calculation of SSZ-24. These results are indicative for an underestimation of the charges used in the partial charge model. The influence of structure on spectra is shown to be rather weak. The main differences between the spectra of $AlPO_4$-5 and SSZ-24 are due to the interatomic force constants.

**Keywords:** Computer simulation; i.r. spectroscopy; Raman spectroscopy; framework; structure determination; ALPO-5, SSZ-24; valence force field

## INTRODUCTION

Since 10 years ago, zeolite chemistry has not been uniquely dealing with (alumino-)silicates, for in 1982, Wilson et al.[1] showed that $AlPO_4$ polymorphs can be formed with topologies similar or equal to those of regular zeolites. One of the early zeolitic $AlPO_4$ polymorphs is $AlPO_4$-5, which has a structure that was not found for ordinary zeolites. After the discovery of the $AlPO_4$'s, silica–alumino–phosphates (SAPOs) were made with the same framework topologies.[2,3] The pure silica analog of $AlPO_4$-5, which is called SSZ-24, was first synthesized by Zones.[4] The SAPO analog of $AlPO_4$-5 exists for silicon-to-aluminum-to-phosphorus ratios of typically 14:45:41.[3]

In the $AlPO_4$-5 structure derived from X-ray diffraction data, large displacements (0.7 Å) of the oxygen atoms from their electron density centers are found.[5] Therefore, a comparison of XRD, neutron diffraction,[6] and theoretical oxygen positions in $AlPO_4$-5 is of interest.

Recently, the SSZ-24 structure was determined by Bialek et al.[7] They explain the fact that SSZ-24 is not formed as easy as is $AlPO_4$-5 by the presence of large T–O–T angles in the structure and the disfavor of silica systems for such angles. Lattice energy calculations can be used to verify this hypothesis.

## METHODS AND MODELS

To investigate the plausibility of a mineral structure, one generally performs lattice energy minimizations.[8–16] Silica polymorphs can be modeled with various readily available atomistic potential parameter sets.[17–20] Two different models for silica will be used here:

- The shell model of Sanders et al.[17,21] containing Coulomb, short-range two-body, and bond-bending terms in combination with a core–shell interaction to simulate the polarizability of the oxygen ions, while for the total charge of each ion the formal value is taken.
- The partial charge model of van Beest et al.[19] with a Coulomb term using partially charged rigid ions and short range two-body terms.

It has been shown before[22,23] that the shell model and the partial charge model, which are parametrized in order to predict structures, are not suitable for calculations of vibrational spectra over the whole fre-

Address reprint requests to Dr. de Man at the Schuit Institute of Catalysis, Eindhoven University of Technology, P.O. Box 513, 5600 MB Eindhoven, The Netherlands.
Received 5 November 1991; accepted 2 March 1992

quency range of interest. Therefore, a generalized valence force field (GVFF[24]) has been applied[25] for the calculation of infrared and Raman spectra of various siliceous polymorphs. This force field has been derived by Etchepare et al.[26] from experimental spectra of α- and β-quartz.

For the modeling of $AlPO_4$'s, a partial charge model, which is consistent with the siliceous partial charge model, has also been developed by van Beest et al.[19] This potential set will be referred to as the ALPO model. Because of the expected limited applicability of the ALPO potential for calculations of vibrational spectra as for silica, a GVFF set is derived that is based on the experimental infrared and Raman spectra of α-berlinite, the $AlPO_4$ analog of α-quartz. Choi et al.[27] derived an $AlPO_4$ potential based on the electronegativity equalization method[28,29] and the constraint method. In the latter method, the potential parameters are chosen such that they reproduce the experimental structure. Choi et al. derived separate potential parameters for every T–O pair in $AlPO_4$-5, thereby limiting the transferability of their parameter set. Therefore, this set will not be used here.

Lattice energy minimizations are done with the THBREL code.[9,10,30] A "constant pressure" relaxation was performed, i.e., the unit cell vectors as well as the atom positions are changed to minimize the lattice energy. No symmetry constraints are used in the relaxation. Ewald summations are applied for the Coulomb term in the energy but the short-range terms are calculated only within a region of 10 Å around each atom of the unit cell.

An $AlPO_4$-5 structure derived by Bennett et al.[5] from powder X-ray diffraction data is used as a starting structure for the lattice energy minimization of $AlPO_4$-5. The structure has a $C_{6v}^2$ symmetry and unit cell axes $a = 13.726$ and $c = 8.484$ Å. At the time of our research, no structural data for SSZ-24 were available, except for the symmetry and unit cell dimensions (13.62 and 8.324 Å, after calcination) given by Zones.[4] The crystallographic positions from a powder neutron diffraction experiment on $AlPO_4$-5 by Richardson et al.,[6] who makes no distinction between aluminum and phosphorus, are used. This requires $D_{6h}^2$ symmetry. Later Bialek et al.[7] determined from XRD experiments a structure with a $D_{6h}^2$ symmetry and cell constants of 13.671 and 8.328 Å. However, two of the oxygen sites were half-occupied, so the actual symmetry is lower.

Phonon calculations in the harmonic approximation[31] using the shell and partial charge models were performed with the THBPHON program[21,31] for wave vectors of about 0.001 reciprocal unit cell length in the $x$ and $z$ direction, representing modes that are detectable by infrared and Raman spectroscopy. Infrared line intensities are calculated from the change in dipole moment that is caused by the vibrational displacement of ionic charges.[32] Raman intensities are calculated using isotropic bond polarizabilities derived from atomic displacements by a method described by Kleinman and Spitzer.[32] For all spectral peaks, line widths of 10 $cm^{-1}$ and a Gaussian line shape were assumed.

Calculations and fitting of spectra using a GVFF are performed with the VIBRAT program of Dowty.[33,34] The program uses the harmonic approximation for zero wave vector modes. Symmetry is explicitly used for solving the dynamical matrix. As for THBPHON, infrared line strengths are calculated using formal ionic charges. These charges are not used as part of the valence force field; they are only added to the model for calculating the change in dipole moment induced by the infrared active vibrational modes. Raman intensities for parallel and crossed polarization are computed by a procedure using differential bond-polarizability tensors with empirical values for spherical part and anisotropy of the polarizability[33,34] and for the relative bond polarizability factors. The force constants in the GVFF set for $AlPO_4$ are fitted using the VIBRAT program and the spectral data for α-berlinite given in *Table 1*. The α-berlinite structure given by Thong and Schwarzenbach[39] has been used for the fitting without any prior structural relaxation. To obtain a valid force field, VIBRAT requires for each group theoretical species at least a selection of modes forming a continuous set, starting at the highest frequency. When such a selection is not possible, all modes belonging to such a representation have to be excluded from the fit. For the least-squares fit, the highest calculated frequency is linked to the highest observed one with the same irreducible representation, and so on. Therefore, all high-frequency modes of a given species have to be known. This limits the fit of GVFF force fields using VIBRAT to well-known crystalline systems or molecules such as α-quartz and α-berlinite.

Vibrational spectra of $AlPO_4$-5 and SSZ-24 are calculated using structures that are relaxed by the partial charge or shell model potentials. The actual spectra are calculated with the $SiO_2$ and $AlPO_4$ GVFF force fields.

## EXPERIMENTAL

Infrared spectra of $AlPO_4$-5 and SSZ-24 were obtained using a Bruker Model 113-v Fourier transform spectrometer with the KBr disc technique. $AlPO_4$-5 and SSZ-24 were synthesized according to U.S. patents 4.310.440 and 4.665.110, respectively. The as-synthesized materials were washed, dried at 120°C for 16 h, and then slowly calcined (with a heating rate of 10°C/min) at 550°C for 2 h. Powder XRD analysis showed no detectable trace of other crystalline materials.

## RESULTS

A group theoretical analysis of α-berlinite, which is similar to the one given before[22] for α-quartz, shows that 12 peaks are to be expected in the stretching frequency region (above 650 $cm^{-1}$) for both the Raman and the infrared spectra. The force constants

**Table 1** Frequencies ($cm^{-1}$) of transversal optical modes of Berlinite

| | Experiment | | | | | Calculated | | |
|---|---|---|---|---|---|---|---|---|
| Ref.: | 35 | | 36 | 37 | 38 | This work | This work | 38 |
| Method[a] | R | I | I | R | I,R | GVFF | ALPO | VFF |
| $A_1$ | 1207 | | | – | 1110[b] | 1132 | 1229 | 1102 |
| | 1106 | | | 1105 | 1103[b] | 1094 | 1078 | 1103 |
| | 727 | | | 729 | 726[b] | 746 | 698 | 773 |
| | 459 | | | 456 | 461[b] | 475 | 567 | 453 |
| | | | | – | 435[b] | 409 | 561 | 387 |
| | 334 | | | 336 | 335[b] | 332 | 390 | 360 |
| | 218 | | | 216 | 221[b] | 220 | 228 | 221 |
| | 160 | | | 158 | 162[b] | 156 | 183 | 211 |
| | 135 | | | | | | | |
| $A_2$ | – | 1158 | 1160 | | 1167[b] | 1146 | 1100 | 1110 |
| | – | 1101 | 1095 | | 1108[b] | 1144 | 1082 | 1106 |
| | – | 688 | 684 | | 691[b] | 686 | 703 | 792 |
| | – | 680[b] | – | | – | 669 | 681 | 783 |
| | 494 | 490 | 515 | | 495[b] | 498 | 565 | 509 |
| | 450 | 440 | 375 | | 447[b] | 427 | 521 | 389 |
| | 273 | 270 | – | | 277[b] | 263 | 377 | 358 |
| | – | – | 140 | | 149[b] | 144 | 193 | 167 |
| | – | – | 48 | | 48[b] | 12 | 54 | 52 |
| $E$ | 1228 | 1229 | 1228 | 1231 | 1231[b] | 1155 | 1215 | 1109 |
| | 1198 | 1186 | 1180 | – | 1171[b] | 1142 | 1197 | 1108 |
| | – | 1130 | 1130 | 1125 | 1125[b] | 1135 | 1091 | 1100 |
| | 1102 | 1101 | 1100 | 1100 | 1096[b] | 1083 | 1078 | 1081 |
| | 748 | 747 | 738 | – | 739[b] | 731 | 801 | 782 |
| | 703 | 705 | 710 | 713 | 706[b] | 682 | 801 | 771 |
| | 650 | 646 | 650 | 697 | 645[b] | 637 | 666 | 701 |
| | 565 | – | – | – | 566[b] | 541 | 637 | 563 |
| | 463 | 468 | 473 | – | 467[b] | 472 | 556 | 474 |
| | 437 | 448 | – | 460 | 438[b] | 445 | 552 | 470 |
| | 417 | 418 | 414 | 417 | 413[b] | 409 | 511 | 410 |
| | 371 | 378 | 379 | 371 | 373[b] | 342 | 438 | 363 |
| | 305 | – | 285 | 296 | 286[b] | 285 | 327 | 261 |
| | 193 | – | 198 | 192 | 193[b] | 196 | 252 | 241 |
| | 160 | – | 165 | – | 157[b] | 142 | 187 | 177 |
| | 115 | – | 126 | 116 | 126[b] | 119 | 147 | 144 |
| | 104 | – | 112 | 105 | 112[b] | 96 | 115 | 119 |

[a] R = Raman; I = infrared
[b] Used to obtain GVFF

**Table 2** Parameters of the GVFFs for $SiO_2$ (Ref. 26) and $AlPO_4$

| $SiO_2$ | | $AlPO_4$ | | |
|---|---|---|---|---|
| $K_{Si-O}$ | 5.943 | $K_{Al-O}$ | 4.197 | mdyn/Å |
| | | $K_{P-O}$ | 5.145 | mdyn/Å |
| $K_{O-Si-O}$ | 0.729 | $K_{O-Al-O}$ | 0.412 | mdynÅ/rad$^2$ |
| | | $K_{O-P-O}$ | 0.998 | mdynÅ/rad$^2$ |
| $K_{Si-O-Si}$ | 0.126 | $K_{Al-O-P}$ | 0.197 | mdynÅ/rad$^2$ |
| $K_{Si-O-Si-O}$ | 0.0056 | $K_{P-O-Al-O}$ | [a] | mdynÅ/rad$^2$ |
| | | $K_{Al-O-P-O}$ | [a] | mdynÅ/rad$^2$ |
| $K_{O-Si,Si-O}$[b] | 0.711 | $K_{O-Al,Al-O}$[b] | 0.594 | mdyn/Å |
| | | $K_{O-P,P-O}$[b] | 0.195 | mdyn/Å |
| $K_{Si-O,O-Si}$ | 0.843 | $K_{Al-O,O-P}$ | −0.438 | mdyn/Å |
| $K_{O-Si,O-Si-O}$[b] | −0.263 | $K_{O-Al,O-Al-O}$[b] | −0.014 | mdyn/rad |
| | | $K_{O-P,O-P-O}$[b] | −0.122 | mdyn/rad |
| $K_{Si-O,Si-O-Si}$ | 0.398 | $K_{Al-O,Al-O-P}$ | [a] | mdyn/rad |
| | | $K_{P-O,Al-O-P}$ | [a] | mdyn/rad |
| $K_{O-Si-O,O-Si-O}$[b] | −0.167 | $K_{O-Al-O,O-Al-O}$[b] | −0.099 | mdynÅ/rad$^2$ |
| | | $K_{O-P-O,O-P-O}$[b] | −0.272 | mdynÅ/rad$^2$ |

[a] This term is not used in the $AlPO_4$ GVFF potential
[b] This interaction is solely calculated for internal coordinates with only the T atom in common

resulting from the fit are given in *Table 2*, together with the force constants for silica derived by Etchepare et al.[26] The resulting frequencies are given in *Table 1*. Infrared spectra for various values of the aluminum/oxygen charge ratio are shown in *Figures 1* and *2* for the ALPO and the GVFF potentials, respec-

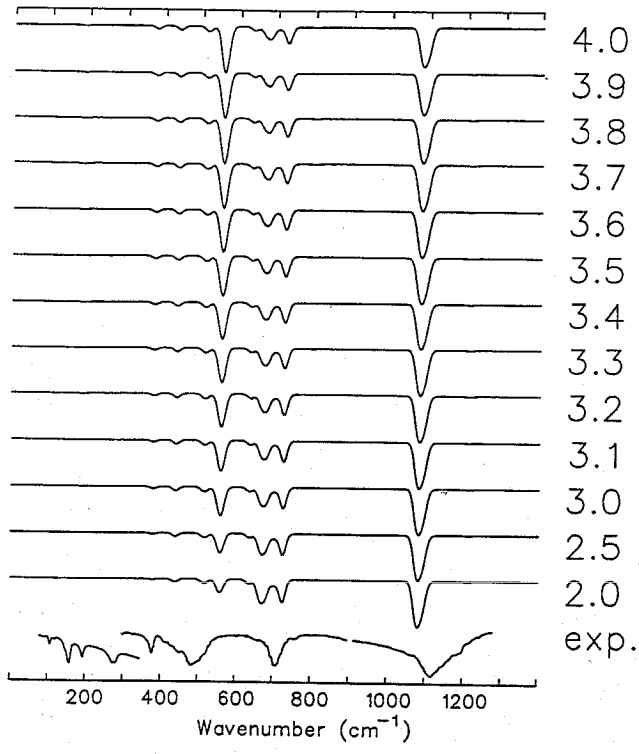


**Figure 1** Calculated and experimental[40] infrared spectra of α-berlinite as a function of the aluminum charge used in the calculation of intensities. The oxygen charge is kept constant at −2. Phonon calculations are done with the ALPO partial charge model using a Coulomb charge of 1.4 for aluminum and −1.2 for oxygen.

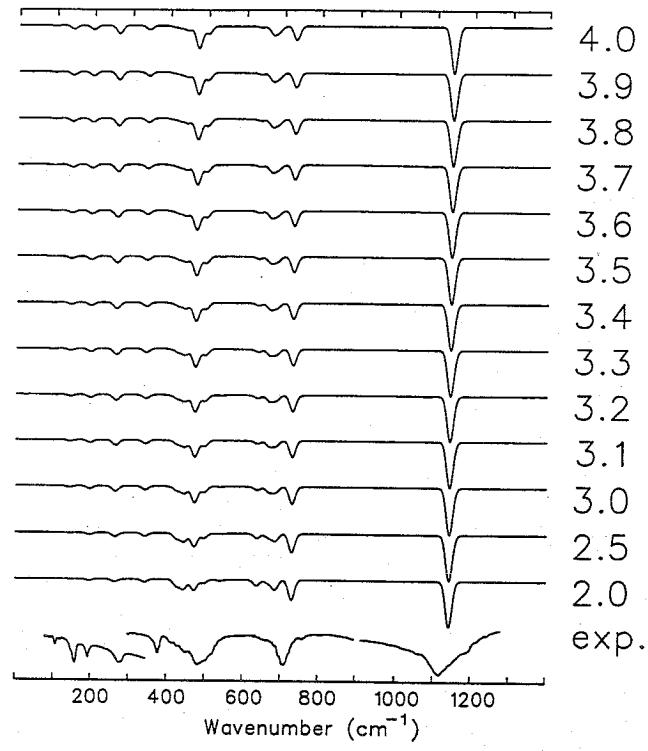


**Figure 2** Calculated and experimental[40] infrared spectra of α-berlinite as a function of the aluminum charge used in the calculation of intensities. The oxygen charge is kept constant at −2. Phonon calculations are done with the GVFF model.

tively. The experimental infrared transmission spectrum in these figures is obtained from data given by Rey[40] (high frequency) and Nyquist and Kagel.[41] From these spectra, one can derive an optimal value of about 1.5 for the aluminum/oxygen charge ratio. This is equal to the ratio of the charges in the ALPO potential. The O–Si–O bending peak (500 cm$^{-1}$) is most sensitive to the charges in our ionic dipole moment model.

The Raman spectra calculated with the GVFF model and experimental spectra[42] are given in *Figure 3*. In this case, intensities depend on the ratio between the polarizabilities of the Al–O and P–O bonds. The peaks at 218 and 459 cm$^{-1}$ in the *zz* Raman spectrum (selective for $A_1$ modes) are not sensitive to this ratio. From the intensity ratio of the peaks at 1106 and 459 cm$^{-1}$, one can derive an Al–O to P–O bond polarizability ratio of 0.5 or 1.5, but it is not clear which of these values has to be preferred.

The relaxation of $AlPO_4$-5 provided a hexagonal structure with the same symmetry as the original structure but with strongly increased unit cell dimensions. A phonon calculation for a small wave vector showed the presence of two imaginary vibrational modes at 25 cm$^{-1}$, indicating that the relaxation was forced by symmetry to end on a saddle point, although it was not formally constrained to the original symmetry. This structure will be called $AlPO_4$-$5_1$. Adding the imaginary modes to the relaxed structure

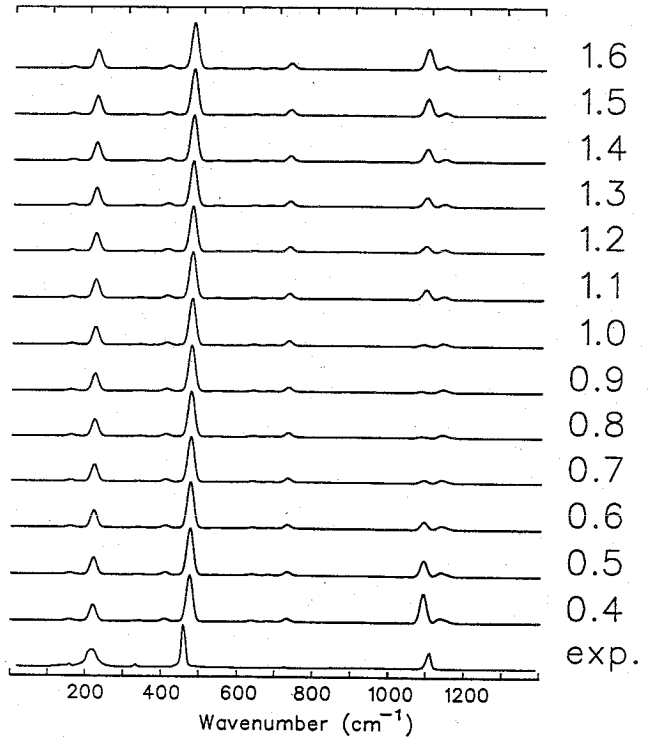


**Figure 3** Calculated and experimental[42] Raman spectra of α-berlinite as a function of the Al–O bond polarization relative to P–O. Phonon calculations are done with the GVFF model.

and relaxing again results in a structure with a lower lattice energy and without imaginary vibrational modes. This structure will be called $AlPO_4$-$5_2$. Its unit

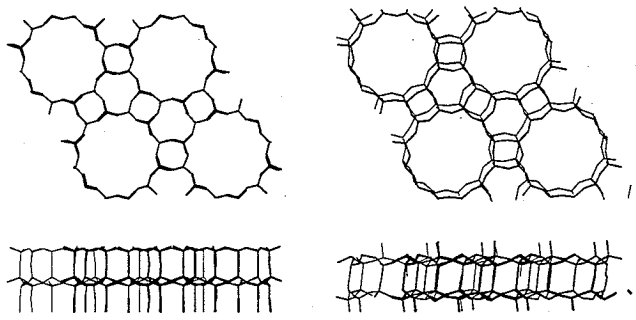

**Figure 4** Experimental and relaxed ($AlPO_4$-$5_2$) structures of $AlPO_4$-5.

cell vectors deviate slightly from those required for hexagonal symmetry. The original and the $AlPO_4$-$5_2$ structure are drawn in *Figure 4*. Some of their properties are listed in *Table 3*.

To test the influence of the experimentally found displacement of O(2),[5,43] a hypothetical $AlPO_4$-5 structure is relaxed. Initially, this structure has $C_{2v}^{12}$ symmetry. The original crystallographic positions as given by Bennet et al. are used except for O(2), which is placed on three positions reflecting peaks in the Fourier difference plot given by Bennet et al. (figure 3 of Ref. 5). These O(2) positions are (0.4300,0.0729,0.75), (0.2710,0.4210,0.75), and (0.1426,−0.3804,0.75) and change the average T–O(2)–T angle from 178° to 131° and the global average Al–O–P angle from 157° to 150°. Relaxation of this test structure results in the previously found $AlPO_4$-$5_1$ structure, which does not represent a real energy minimum.

The result of applying the $C_{6v}^2$ symmetry operations on the oxygen positions of the double relaxed $AlPO_4$-$5_2$ structure is shown in *Figure 5*, together with the original positions. In contradiction to the experiment, the O(2) positions obey the $C_{6v}^2$ symmetry better than do the other oxygen sites. This deviation is caused by the shift of layers in the $AlPO_4$-$5_2$ structure of about $0.048 \cdot a$, which affects all but the O(2) atoms. The O(2) atoms occupy positions between the two layers, while the oxygen atoms on the other crystallographic sites appear inside both layers.

The relaxation of pure silica SSZ-24 shows the same peculiarities as the $AlPO_4$-5 relaxation. The lattice energy minimizations using both silica potentials with atomic positions and symmetry of the $AlPO_4$-5 structure of Richardson et al.[6] and unit cell dimensions given by Zones[4] result in highly symmetric structures with imaginary vibrational modes. We will call these structures SSZ-$24_{1P}$ (partial charge model) and SSZ-$24_{1S}$ (shell model). Relaxing these relaxed structures after deformation by an imaginary vibrational mode results in low-symmetry stabilized structures, which we will refer to as SSZ-$24_{2P}$ and SSZ-$24_{2S}$. A summary of results from the minimizations is given in *Tables 4* and *5* and the structures are drawn in *Figures 6* and *7*.

The increase of the unit cell dimensions, especially the *a* value, relative to the values given by Zones agrees with the findings of Bialek et al.[7] Only the SSZ-$24_{2S}$ structure deviates from this. It has been seen before[17,19,23,44] that the shell model usually gives unit cells that are too small. The tetrahedral angles in the structures obtained from the partial charge model are more distorted than those obtained from the shell model. This is due to the presence of the three-body bending term in the shell model. However, the effect of this term should not be overestimated: The energetically most favorable shell model structure (SSZ-$24_{2S}$) shows a larger deformation of the tetrahedral angles than the less favorable SSZ-$24_{1S}$. Another striking difference between the partial charge and the shell model is the magnitude of the Si–O–Si angles. The partial charge model gives larger angles. Even an angle of 180° is present in the SSZ-$24_{1P}$ and SSZ-$24_{2P}$ structures. As for $AlPO_4$-5, a shift of layers occurs in partial charge model relaxed SSZ-24. This shift amounts to $0.067 \cdot a$, but is not present in the shell model. To avoid an oxygen site with a Si–O(2)–Si angle close to 180°, Bialek et al.

**Table 3** Results of the lattice energy minimization of $AlPO_4$-5

| | Experiment | | Calculated | | |
|---|---|---|---|---|---|
| | Ref. 5 | Ref. 6[a] | $AlPO_4$-$5_1$ | $AlPO_4$-$5_2$ | |
| Energy: | – | – | −5688.92 | −5690.05 | kJ/mol $TO_2$ |
| Symmetry: | $C_{6v}^2$ | $C_{6v}^2$ | $C_{6v}^2$ | $C_s^4$ | |
| *a* | 13.736 | 13.771 | 14.183 | 13.979[b] | Å |
| *c* | 8.484 | 8.379 | 8.678 | 8.425 | Å |
| ‹Al–O› | 1.710 | 1.595 | 1.747 | 1.747 | Å[c] |
| Al–O | 1.683 . . . 1.729 | 1.559 . . . 1.632 | 1.735 . . . 1.761 | 1.728 . . . 1.768 | Å |
| ‹P–O› | 1.486 | 1.595 | 1.509 | 1.509 | Å[c] |
| P–O | 1.456 . . . 1.525 | 1.559 . . . 1.632 | 1.449 . . . 1.519 | 1.497 . . . 1.521 | Å |
| ‹Al–O–P› | 157.0 | 154.9 | 162.6 | 158.5 | °[c] |
| ‹Al–O–P› | 148.8 . . . 178.1 | 146.6 . . . 176.1 | 153.9 . . . 178.4 | 144.2 . . . 178.7 | ° |
| $\sigma_{Al}$ | 2.747 | 2.583 | 2.963 | 3.464 | °[d] |
| $\sigma_P$ | 1.307 | 2.583 | 1.886 | 1.972 | °[d] |

[a] In Ref. 6, no distinction between Al and P is made
[b] Average value: $a = 13.8201$ and $b = 14.1375$
[c] Average is taken over Wyckoff sites, not over atoms
[d] $\sigma_T$ values are root mean square deviations from the ideal tetrahedron angle

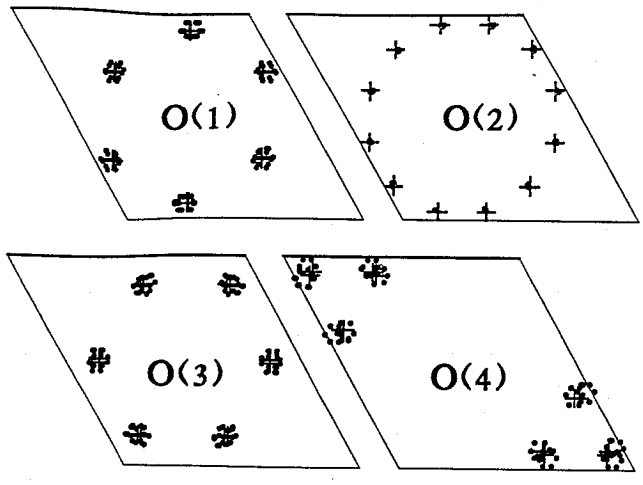


**Figure 5** Oxygen sites in $AlPO_4$-5 viewed along the *c* axis. The crosses are the unrelaxed positions; the dots result from applying the symmetry operations of the original structure on the oxygen atoms of the $AlPO_4$-$5_2$ structure. Each drawing represents a Wyckoff site.

used two half-occupied crystallographic sites for O(2) at a mutual distance of 0.57 Å. The average site of the two gives a Si–O–Si angle of 175°. The experimental temperature factors of the two O(2) sites are still high compared to those of the other oxygen atoms. In their powder neutron diffraction experiment on SSZ-24, Richardson et al. observed a high-low phase transition at 370 K. In the Fourier difference map of the low-temperature phase, three peaks for O(2) were observed, just as for $AlPO_4$-5. At high temperatures, the three peaks join in a large peak that is circular in cross section. The Si–O(2)–Si angle changed from below 170° at room temperature to 176.5° at 368 K and 179.4° at 464 K. Note that Bialek et al.[7] use in their structure determination of SSZ-24 the label O(4) for the O(2) atom in $AlPO_4$-5.

Using the double relaxed structures $AlPO_4$-$5_2$, SSZ-$24_{2P}$, and SSZ-$24_{2S}$ and the ALPO and GVFF force fields vibrational spectra are calculated. These calculated spectra and experimental infrared spectra of $AlPO_4$-5 and SSZ-24 are shown in *Figures 8* to *10*. The main difference between the experimental $AlPO_4$-5 and SSZ-24 infrared spectra is the number of peaks between 500 and 900 $cm^{-1}$ and the position of the

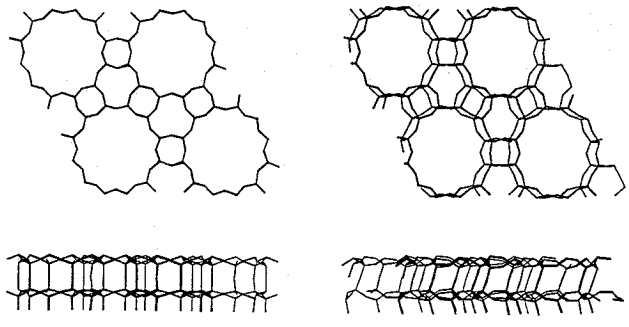

**Figure 6** Experimental and partial charge relaxed (SSZ-$24_{2P}$) structures of SSZ-24.

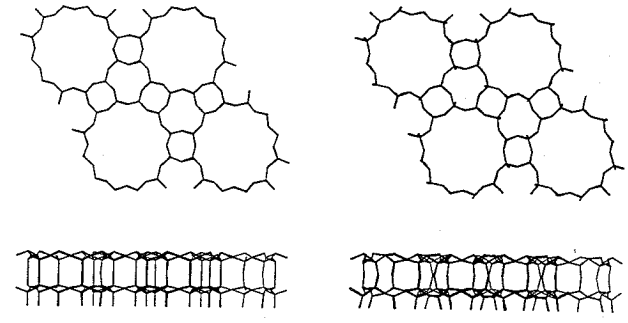

**Figure 7** Experimental and shell model relaxed (SSZ-$24_{2S}$) structures of SSZ-24.

symmetric stretching peak (705 $cm^{-1}$ for $AlPO_4$-5 and 805 $cm^{-1}$ for SSZ-24). The frequencies of asymmetric stretching peaks differ much less (1132 $cm^{-1}$ for $AlPO_4$-5 vs. 1105 $cm^{-1}$ for SSZ-24) and the bending peaks are virtually the same. The double relaxation has an important effect on the frequencies of the spectra. This is due mainly to the change of T–O–T angles. The atomic displacement vectors of the vibrational modes of the single and double relaxed structures, however, are very similar. This is shown in *Figure 11*, which gives the square of the projection of the infrared active vibrational modes of the double relaxed structure $AlPO_4$-$5_2$ on the modes of the single relaxed structure $AlPO_4$-$5_1$. For the SSZ-$24_P$ structures, a similar picture is obtained.

To investigate the influence of structural features on infrared spectra, calculations are done with a silicon-substituted $AlPO_4$-$5_2$ structure using the silica GVFF potential and an $AlPO_4$-substituted SSZ-$24_{2P}$ structure using the $AlPO_4$ GVFF potential (*Figure 12*). The contribution of various tetrahedron modes on the crystal vibration is also expressed as a projection value in *Figures 13–15*. One observes that only in the high-frequency region, around 1100 $cm^{-1}$, crystal modes can be correlated with unique tetrahedron modes. The figures also clearly illustrate the decrease of the importance of the asymmetric (high frequency $T_2$) and especially the symmetric ($A_1$) tetrahedron stretching modes with decreasing frequency of the crystal mode.[25] The most striking feature of the three figures is the difference of behavior of the $PO_4$ $A_1$-mode compared with the $SiO_4$ and $AlO_4$ $A_1$-modes. Because the calculated frequency of the molecular $T_2$ stretching mode of $PO_4$ is significantly larger than the corresponding value for $AlO_4$ (960 vs. 847 $cm^{-1}$), one should expect the contribution of $PO_4$ $T_2$-modes to the highest crystal frequencies to be larger than that of $AlO_4$, but the reverse is observed. This may be due to the weak $K_{O-P,P-O}$ interaction term compared with $K_{O-Al,Al-O}$ and $K_{O-Si,Si-O}$.

## DISCUSSION AND CONCLUSION

The quality of the GVFF found for berlinite is satisfying and comparable with Etchepare's GVFF parameter set for silica, as can be seen from the root mean square deviations of the frequencies in *Table 6*.

**Table 4** Results of the lattice energy minimization of SSZ-24 using the partial charge model

| | Experiment | | Calculated | | |
|---|---|---|---|---|---|
| | [a] | Ref. 7 | $SSZ\text{-}24_{1P}$ | $SSZ\text{-}24_{2P}$ | |
| Energy: | – | – | −5590.25 | −5592.39 | kJ/mol $SiO_2$ |
| Symmetry: | $C^2_{6v}$ | $D^2_{6h}$ | $C^2_{6v}$ | $C^4_s$ | |
| *a* | 13.62 | 13.671 | 13.995 | 13.712[b] | Å |
| *c* | 8.324 | 8.328 | 8.565 | 8.194 | Å |
| ‹Si–O› | 1.580 | 1.599 | 1.606 | 1.605 | Å[c] |
| Si–O | 1.543 . . . 1.615 | 1.576 . . . 1.621 | 1.596 . . . 1.616 | 1.591 . . . 1.621 | Å |
| ‹Si–O–Si› | 154.9 | 151.3 | 163.0 | 157.5 | °[c] |
| Si–O–Si | 146.7 . . . 176.2 | 142.2 . . . 164.7 | 153.6 . . . 178.2 | 140.8 . . . 179.9 | ° |
| $\sigma_{Si}$ | 2.544 | 6.468 | 2.545 | 3.016 | °[d] |

[a] Unit cell dimensions from Ref. 4 and positions and symmetry from Ref. 6
[b] Average value: $a = 13.934$ and $b = 13.490$
[c] Average is taken over Wyckoff sites, not over atoms
[d] $\sigma_{Si}$ values are root mean square deviations from the ideal tetrahedron angle

**Table 5** Results of the lattice energy minimization of SSZ-24 using the shell model

| | Experiment | | Calculated | | |
|---|---|---|---|---|---|
| | [a] | Ref. 7 | $SSZ\text{-}24_{1S}$ | $SSZ\text{-}24_{2S}$ | |
| Energy: | – | – | −12406.17 | −12407.25 | kJ/mol $SiO_2$ |
| Symmetry: | $C^2_{6v}$ | $D^2_{6h}$ | $D^2_{6h}$ | $C^1_6$ | |
| *a* | 13.62 | 13.671 | 13.685 | 13.602 | Å |
| *c* | 8.324 | 8.328 | 8.464 | 8.311 | Å |
| ‹Si–O› | 1.580 | 1.599 | 1.596 | 1.604 | Å[b] |
| Si–O | 1.543 . . . 1.615 | 1.576 . . . 1.621 | 1.585 . . . 1.604 | 1.542 . . . 1.672 | Å |
| ‹Si–O–Si› | 154.9 | 151.3 | 156.1 | 146.7 | °[b] |
| Si–O–Si | 146.7 . . . 176.2 | 142.2 . . . 164.7 | 148.2 . . . 177.4 | 141.0 . . . 155.0 | ° |
| $\sigma_{Si}$ | 2.544 | 6.468 | 1.471 | 2.173 | °[c] |

[a] Unit cell dimensions from Ref. 4 and positions and symmetry from Ref. 6. Powder neutron diffraction data of Richardson et al[39] gives $a = 13.6386$ and $c = 8.3071$
[b] Average is taken over Wyckoff sites, not over atoms
[c] $\sigma_{Si}$ values are root mean square deviations from the ideal tetrahedron angle

As in Etchepare's model, the *E*-modes show the largest discrepancy. Inclusion of torsion terms $K_{P\text{–}O\text{–}Al\text{–}O}$ and $K_{Al\text{–}O\text{–}P\text{–}O}$ will give only small improvements in the low-frequency region. The inclusion of the stretching–bending interaction terms $K_{Al\text{–}O,Al\text{–}O\text{–}P}$ and $K_{P\text{–}O,Al\text{–}O\text{–}P}$ is tested but did not result in a significant improvement.

The P–O stretching force constant was expected to be higher than the one for Al–O, which is indeed found in our fitting procedure, but the value we

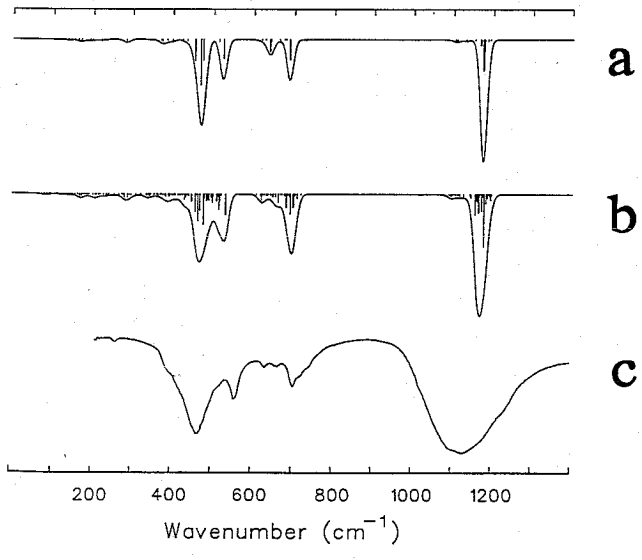


**Figure 8** Calculated and experimental infrared spectra of $AlPO_4$-5. Phonon calculations are done with the GVFF model on the (a) $AlPO_4\text{-}5_1$ and (b) $AlPO_4\text{-}5_2$ structure.

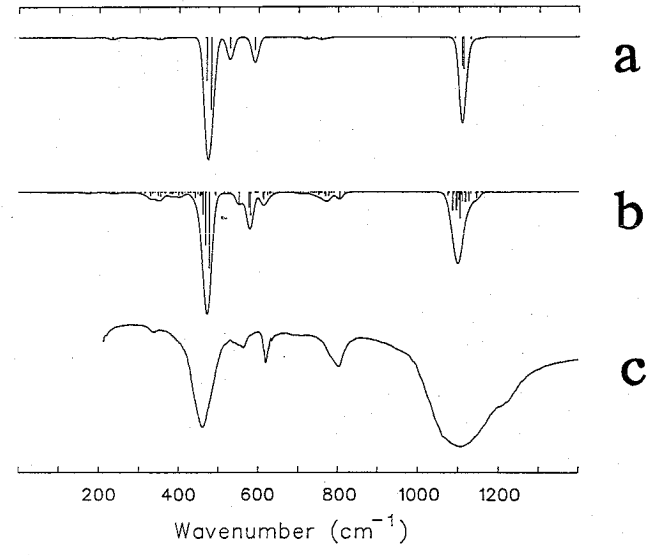


**Figure 9** Calculated and experimental infrared spectra of SSZ-24. Phonon calculations are done with the GVFF model on the (a) $SSZ\text{-}24_{1P}$ and (b) $SSZ\text{-}24_{2P}$ structure.

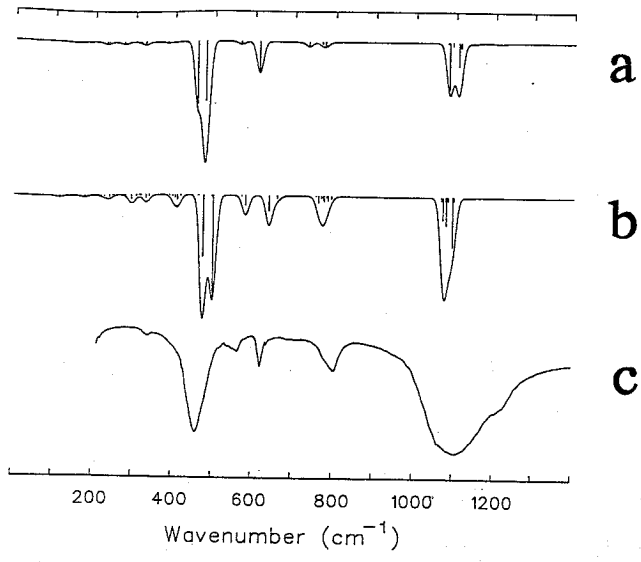


**Figure 10** Calculated and experimental infrared spectra of SSZ-24. Phonon calculations are done with the GVFF model on the (a) SSZ-$24_{1s}$ and (b) SSZ-$24_{2s}$ structure.

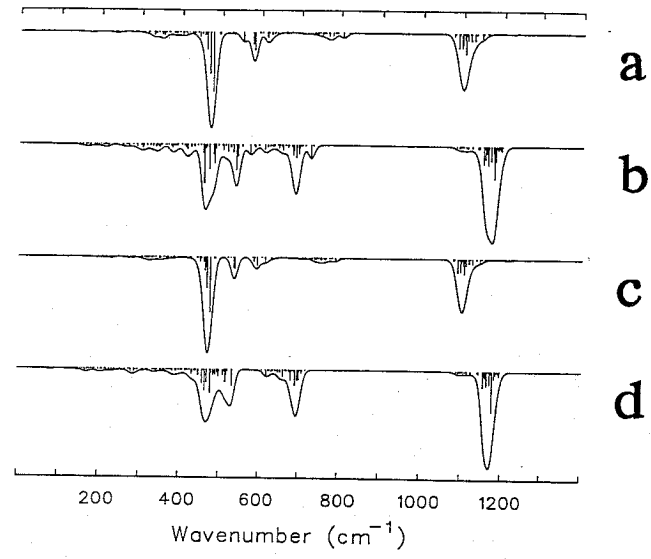


**Figure 12** Calculated infrared spectra of (a) SSZ-$24_{2P}$, (b) $AlPO_4$-substituted SSZ-$24_{2P}$, (c) silica-substituted $AlPO_4$-$5_2$, and (d) $AlPO_4$-$5_2$.

found is lower than the one for $SiO_4$, which is contrary to expectation. Lazarev and co-workers tried to obtain some force constants for aluminates[45] and phosphates[46] by a fit on experimental spectra of hydroaluminate ions in high-alkali aqueous solutions. They used spectra of $Al(OH)_4^-$, $(HO)_3AlOAl(OH)_3^{2-}$, crystalline γ-$LiAlO_2$, $PO_4^{3-}$, $Ba_3(PO_4)_2$, and $Sr_3(PO_4)_2$ and presented various sets of force constants. The difference between those sets illustrates the problem of transferability of force field parameters between systems with different stoichiometry. Some of the force constants of this work are listed in *Tables 7* and *8*. The main difference between the force fields in the literature and our parameter set is the value of $K_{P-O}$. To test the validity of our force field, a fit on the previously used α-berlinite spectra was made in which the force constants of Lazarev et al.[46] for $PO_4^{3-}$ were used and all other constants were varied. This did not result in a better fit.

Choi et al.[27] derived a potential set with $K_{Al-O}$ values ranging from 5.896 to 6.401 mdyn/Å, $K_{P-O}$ values from 5.896 to 6.401 mdyn/Å, an O–O Lennard–Jones term, and a general Coulomb term (which influences the effective stretching constants) with charges of 0.29683 for phosphorus, 1.23133 for aluminum, and −0.37189 to −0.40466 for oxygen. O'Keefe et al.[50] gave a much larger value of the $K_{P-O}$ (9.16 mdyn/Å) based on STO–3G* *ab initio* calculations for $H_4P_2O_7$. These calculations are known to give stretching frequencies that are about 10% too high.[51,52] Other force constants given by O'Keefe are 0.69 mdyn/rad for $K_{O-P,P-O-P}$ and 0.47 mdynÅ/rad$^2$ for $K_{P-O-P}$. These two terms are not present in $AlPO_4$'s.

Some of the experimental frequencies used to determine our force constants are subject to discus-

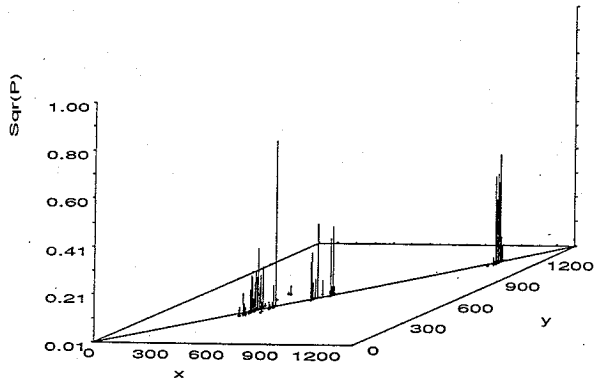


**Figure 11** Infrared active modes of $AlPO_4$-$5_2$ (**x**-axis) projected on all vibrational modes of $AlPO_4$-$5_1$ (**y**-axis). **x** and **y** values are the wavenumbers of the crystal modes in cm$^{-1}$.

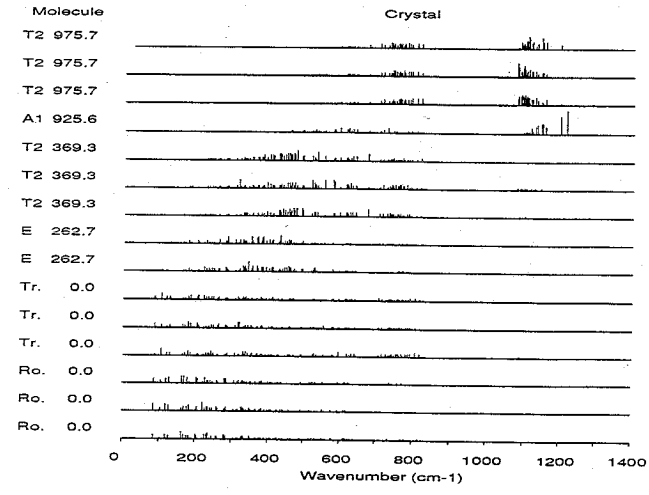


**Figure 13** Projection of infrared active vibrational modes of the SSZ-$24_{2P}$ crystal on all vibrations of a free $SiO_4$ molecule (averaged over all $SiO_4$ tetrahedra of the crystal). The group theoretical assignment and frequencies of molecule modes are given in the column at left. Tr. means translation; Ro. means rotation.

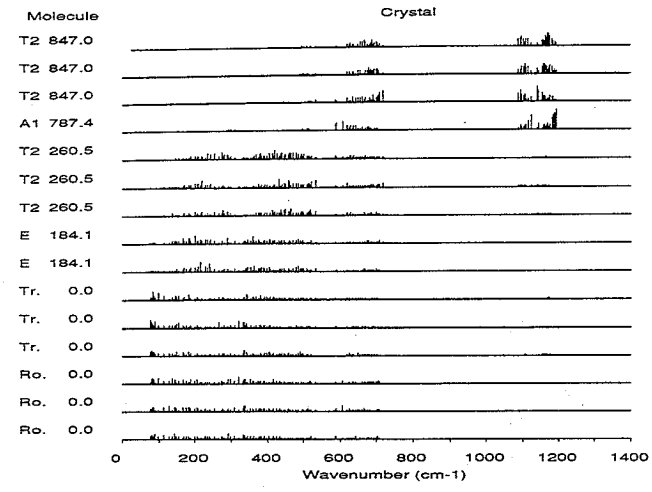


**Figure 14** Projection of infrared active vibrational modes of the $AlPO_4$-$5_2$ crystal on all vibrations of a free $AlO_4$ molecule (averaged over all $AlO_4$ tetrahedra of the crystal). The group theoretical assignment and frequencies of molecule modes are given in the column at left. Tr. means translation; Ro. means rotation.

sion. The peak at 1231 $cm^{-1}$ is very weak and its existence as a transversal optical mode is questionable. The peaks at 680,[35] 684,[36,53] 688,[35] and 691[38] $cm^{-1}$ may be one and the same mode, although they are regarded as double in some assignments. Goullet et al.[38] performed some highly approximate calculations on berlinite using stretching and bending force constants of silica including T–T and O–O interactions. Their calculations did not give two modes in the 680 $cm^{-1}$ region or a mode at 1230 $cm^{-1}$. An estimation of the optical frequencies by Scott[37] also suggested the unlikeliness of a transversal optical mode at 1231 $cm^{-1}$. In his experimental Raman spectrum for *xz* geometry, Scott assigns a peak at 1231 $cm^{-1}$ as TO+LO, whereas his experimental

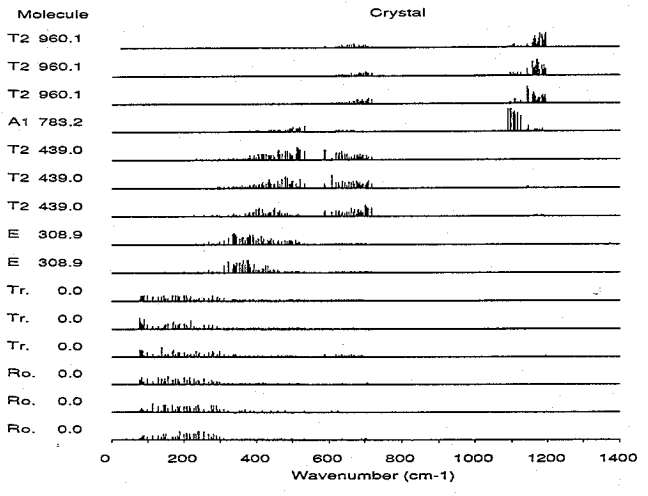


**Figure 15** Projection of infrared active vibrational modes of the $AlPO_4$-$5_2$ crystal on all vibrations of a free $PO_4$ molecule (averaged over all $PO_4$ tetrahedra of the crystal). The group theoretical assignment and frequencies of molecule modes are given in the column at left. Tr. means translation; Ro. means rotation.

**Table 6** Root mean square deviations ($cm^{-1}$) of calculated and experimental optical frequencies for α-quartz[26] and α-berlinite

| | GVFF[26] | | ALPO | |
|---|---|---|---|---|
| Species | *N* | RMS | *N* | RMS |
| $A_1$ | 4 | 12.9 | 8 | 14.8 |
| $A_2$ | 4 | 10.1 | 9 | 20.7 |
| *E* | 8 | 19.4 | 17 | 23.4 |
| All | 16 | 16.0 | 34 | 21.0 |

*N* = number of (degenerate) modes. RMS = root mean square deviation of calculated frequencies from experimental values

Raman spectrum in *zz* geometry, which does not show E(LO) modes and therefore should be used to determine the transversal/longitudinal character of the mode, stops at 1150 $cm^{-1}$. More recent Raman spectroscopic data[42] in *zz* geometry showed only a very weak feature around 1230 $cm^{-1}$. The $A_1$-mode found by Lazarev et al.[35] at 135 $cm^{-1}$ might be an overtone of an acoustic mode.

Based on the TO–LO splitting of vibrational modes, Scott assigned effective charges of 2.2, 2.4, and −1.15 for Al, P, and O, respectively, so giving an aluminum-to-oxygen charge ratio of 1.9. This is not in agreement with our calculations with the ALPO and the GVFF model, which give a value of 1.5 for the charge ratio in the potential as well as for the charges used in intensity calculations. Part of this discrepancy may be caused by the physical difference between TO–LO effective charges (expressing interatomic forces) and charges derived from intensities (expressing an electric field change upon displacement). Uytterhoeven et al[54] applied the electronegativity equalization method[29] on various $AlPO_4$ systems. For α-berlinite, they found charges of 1.396, 1.748, and −0.786 (average) for aluminum, phosphorus, and oxygen, respectively, so giving a charge ratio of 1.78, a value between Scott's and ours.

Of the two bond polarizability ratios that best represent intensities, the lowest one (Al–O/P–O = 0.5) seems to be the most reasonable, as indicated by Dowty[55] who found an Al–O/Si–O bond polarizability ratio of about 0.7 and suggested an increase of bond polarizability with atom number for the third-row elements. It should be noted that the effect of the atomic polarizability (8.34 $Å^3$ for Al, 3.63 $Å^3$ for P, and 0.802 $Å^3$ for O[56]) is ignored. An empirical relation for the mean differential polarizability for the totally symmetric vibration of $XY_4$ tetrahedra is given by Woodward and Long[57]:

$$\bar{\alpha} = \text{const.}(Z_x - Z_y)\exp[-\frac{1}{4}(\chi_x - \chi_y)^2]$$

where $\chi_x$ = Pauling electronegativity ($\chi_{Al}$ = 1.61; $\chi_{Si}$ = 1.90; $\chi_P$ = 2.19; $\chi_O$ = 3.44)[58], and $Z_x$ = atom number. This results in an $AlO_4/PO_4$ polarizability ratio of 0.58, which is in close agreement with the lower value of our bond polarizability estimates. The $AlO_4/SiO_4$ ratio of 0.69 is also in good agreement with

**Table 7** Comparison with literature of GVFF parameters involving aluminum

| Ref.: | This work | 47 | 47 | 45 | |
|---|---|---|---|---|---|
| System: | α-Berlinite | $Al(OH)_4^-$ | $Al(OH)_4^-$ | $Al_2O_7H_6^{2-}$ | |
| Method: | Fit | MNDO | BR[a] | Fit | |
| $K_{Al-O}$ | 4.197 | 4.11 | 2.89 | 3.594 | mdyn/Å |
| $K_{O-Al-O}$ | 0.412 | 1.32 | 1.24 | 0.88 | mdynÅ/rad² |
| $K_{O-Al,Al-O}$ | 0.594 | 0.20 | – | 0.24 | mdyn/Å |
| $K_{O-Al,O-Al-O}$ | −0.014 | −0.128 | – | – | mdyn/rad |
| $K_{O-Al-O,O-Al-O}$ | −0.099 | 0.41 | – | – | mdynÅ/rad² |

[a] Badger's rule[48,49]

the empirical findings of Dowty for the corresponding bond polarizability ratio.

In agreement with experimental observations[5] on $AlPO_4$-5, our lattice energy minimizations indicate that the symmetry of $AlPO_4$-5 is lower than hexagonal. However, the way the structure deforms is completely different from that in the experimental case. Experimentally, the oxygen atoms O(2) showed large displacements from the centroid, whereas in our calculations, all but the O(2) atoms deviate from hexagonal symmetry and the structure shows a shift of layers in the unit cell. A similar result applies for the energy minimization of SSZ-24 using the silica partial charge model. The silica shell model, however, does not show a shift. This gives rise to the question whether the layer shift is real or a typical artifact of the partial charge $AlPO_4$ and $SiO_2$ models. These two models were not derived individually, so they can have some common defects. The lower symmetry of $AlPO_4$-5 is not supported by $^{31}P$ n.m.r. measurements of Blackwell and Patton[59] and Müller et al.,[60] which show a single peak at −27.8 and −29.2 ppm, respectively (relative to 85% $H_3PO_4$) with a half-width of 650 Hz and only a minor asymmetry for calcined $AlPO_4$-5. The application of static and $^{27}Al$ *MAS* n.m.r. to ALPOs is complicated because second-order quadrupole effects are dominant,[59–61] so no decisive information on the symmetry question can be obtained from $^{27}Al$ n.m.r. experiments. The average Al–O–P angles for the experimental structure of Bennet et al.[5] (without correction for the oxygen displacements) and the relaxed $AlPO_4$-$5_2$ structure are almost equal (see *Table 3*). In the experimental structure of Richardson et al.,[6] the Al–O–P angle is somewhat smaller and more in agreement with the 150° derived by Müller et al.[57] from $^{31}P$ and $^{27}Al$ *MAS* n.m.r. experiments. The larger distortion of the tetrahedral angles for aluminum than for phosphorus (the $\sigma_T$ values in *Table 3*) is also confirmed by n.m.r.[60] The observed higher symmetry of the experimental structures compared to that of the structures predicted on the basis of the partial charge models is indicative for an underestimation of the atomic charges. Analyses of structural changes caused by different potential parameter sets have demonstrated a stabilization of symmetrical structures with increasing atomic charge.[15] The higher symmetry of the structure predicted with the shell model seems to confirm this. The lack of an explicit O–T–O bending term in the partial charge potentials, which allows for the distortion of the tetrahedra that is needed for the shift of layers, may also contribute to this. The silica partial charge model, however, has been shown to reproduce O–T–O angles reasonably well.[19,23,44] The T–O–T angles of the partial charge and the shell model are almost the same and the T–O(2)–T angle is close to 180° for both models, so T–O–T angles are not responsible for the difference between the silica partial charge and shell model. Clearly, no disfavor of silica structures for high T–O–T angles is observed, contrary to the hypothesis of Bialek et al.[7]

The calculated infrared spectra show (*Figure 12*) that only minor spectral features are due to structure and that spectra are virtually determined by the chemical composition, i.e., the force constants. The observed nonuniform distribution of $PO_4$ and $AlO_4$ tetrahedron vibrations over the crystal modes illustrates the application of infrared spectroscopy to determine the chemical composition of a crystal. Especially for SAPO systems, calculations like these will be useful. One of the major questions in SAPO research is which T atoms mainly surround silicon. To answer this question, a very sophisticated GVFF is required that probably cannot be determined by a fit on spectra of a reference compound because of the lack of experimental data and usable crystals. The quantum chemical methods that are widely used nowadays to determine force constants suffer from a similar problem: satisfactory calculations can be done only for molecular systems, whereas the force constants usually are intended to be applied to crystals. Therefore, indirect methods using calculations on various simplified structures, like pure silica and pure $AlPO_4$ systems, should be used when investigating complex structures like zeolites, SAPOs, and MeAPOs. The projection of calculated vibrational modes as applied here is one of those methods.

**Table 8** Comparison with literature of GVFF parameters involving phosphorus

| Ref.: | This work | 46 | 46 | |
|---|---|---|---|---|
| System: | α-Berlinite | $PO_4^{3-}$ | $Ba_3(PO_4)_2$ | |
| Method: | Fit | Fit | Fit | |
| $K_{P-O}$ | 5.145 | 6.304 | 6.599 | mdyn/Å |
| $K_{O-P-O}$ | 0.998 | 2.08 | 1.89 | mdynÅ/rad² |
| $K_{O-P,P-O}$ | 0.195 | 0.65 | 0.58 | mdyn/Å |
| $K_{O-P,O-P-O}$ | −0.122 | 0.44 | 0.47 | mdyn/rad |
| $K_{O-P-O,O-P-O}$ | −0.272 | 0.38 | 0.41 | mdynÅ/rad² |

## REFERENCES


1 Wilson, S.T., Lok, B.M., Messina, C.A., Cannan, T.R. and Flanigen, E.M. *J. Am. Chem. Soc.* 1982, **104**, 1146
2 Lok, B.M., Messina, C.A., Patton, R.L., Cannan, T.R. and Flanigen, E.M. *J. Am. Chem. Soc.* 1984, **106**, 6092
3 Flanigen, E.M., Lok, B.M., Patton, R.L and Wilson, S.T., in *New Developments in Zeolite Science and Technology, Proceedings of the 7th International Zeolite Conference, Tokyo, 1986* (Eds. Y. Murahami, A. Lijima and J.W. Ward), p.103
4 Zones, S.I., Eur. Pat. Appl. 231 019 (1987)
5 Bennet, J.M., Cohen, J.P., Flanigen, E.M., Pluth, J.J. and Smith, J.V. ACS Symp. Ser. 218, Am. Chem. Soc., Washington, DC, 1983, p.109
6 Richardson, J.W., Pluth, J.J. and Smith, J.V. *Acta Crystallogr C* 1987, **43**, 1469
7 Bialek, R., Meier, W.M., Davis, M.E. and Annen, M.J. *Zeolites* 1991, **11**, 438
8 Catlow, C.R.A. and Cormack, A.N. *Int. Rev. Phys. Chem.* 1987, **6**, 227
9 Catlow, C.R.A. and Mackrodt, W.C. *Computer Simulation of Solids*, Lecture Notes on Physics, Springer, Berlin, 1982
10 Catlow, C.R.A., Doherty, M., Price, G.D., Sanders, M.J. and Parker, S.C. *Mater. Sci. Forum* 1986, **7**, 163
11 Grant, G.H. and Abrahams, R.J. *Catalysis* 1990, **8**, 68 (A review of recent literature)
12 Lasaga, A.C. and Gibbs, G.V. *Phys. Chem. Minerals* 1987, **14**, 107
13 van Santen, R.A., van Beest, B.W.H. and de Man, A.J.M., in *Guidelines for Mastering the Properties of Molecular Sieves* (Eds. D. Barthomeuf et al.) NATO ASI 221, Plenum, New York, 1990, 201
14 van Santen, R.A., de Man, A.J.M., Jacobs, W.P.J.H., Teunissen, E.H. and Kramer, G.J. *Catal. Lett.* 1991, **9**, 273
15 Kramer, G.J., van Beest, B.W.H. and van Santen, R.A. *Nature* 1991, **351**, 636
16 Kramer, G.J., de Man, A.J.M. and van Santen, R.A. *J. Am. Chem. Soc.* 1991, **131**, 6435
17 Sanders, M.J., Leslie, M. and Catlow, C.R.A. *J. Chem. Soc., Chem. Commun.* 1984, 1271
18 Jackson, R.A. and Catlow, C.R.A. *Mol. Simulation* 1988, **1**, 207
19 van Beest, B.W.H., Kramer, G.J. and van Santen, R.A. *Phys. Rev. Lett.* 1990, **64**, 1955
20 de Vos Burchart, E., Verheij, V.A., van Bekkum, H. and van de Graaf, B. *Zeolites* 1992, **12**, 183
21 Sanders, M.J. PhD Thesis, University of London, 1984
22 de Man, A.J.M., van Beest, B.W.H., Leslie, M. and van Santen, R.A. *J. Phys. Chem.* 1990, **94**, 2524
23 Kramer, G.J., Farragher, N., van Beest, B.W.H. and van Santen, R.A. *Phys. Rev. B* 1991, **43**, 5068
24 Ross, S.D. *Inorganic Infrared and Raman Spectra*, McGraw-Hill, London, 1972
25 de Man, A.J.M. and van Santen, R.A. *Zeolites* 1992, **12**, 269
26 Etchepare, J., Merian, M. and Smetankine, L. *J. Chem. Phys.* 1974, **60**, 1873
27 Choi, K.J., Jhon, M.S. and No, K.T. *Bull. Korean Chem. Soc.* 1987, **8**, 155
28 Huheey, E. *J. Phys. Chem.* 1965, **69**, 3284
29 Mortier, W.J., Ghosh, S.K. and Shankar, S. *J. Am. Chem. Soc.* 1986, **108**, 4315
30 Leslie, M. *Daresbury Laboratory Technical Memorandum*, in preparation
31 Dolling, G., Calculations of phonon frequencies, in *Methods in Computational Physics* (Ed. G. Gilat) Academic Press, London, 1976, Vol. 15.
32 Kleinman, D.A. and Spitzer, W.G. *Phys. Rev.* 1962, **125**, 16
33 Dowty, E. *Phys. Chem. Minerals* 1987, **14**, 67
34 Dowty, E. *VIBRAT Manual*, Bogota, NJ, 1988
35 Lazarev, A.N., Mazhenov, N.A. and Mirgorodskii, A.P. *Opt. Spectrosc.* 1979, **46**, 348
36 Camassel, J., Goullet, A. and Pascual, *J. Phys. Rev. B* 1988, **38**, 8419
37 Scott, J.F. *Phys. Rev. B* 1971, **4**, 1360
38 Goullet, A., Bretagnon, T., Camassel, J. and Pascual, J. *Phys. Scr.* 1990, **42**, 478
39 Thong, N. and Schwarzenbach, D. *Acta Crystallogr. A* 1979, **35**, 658
40 Rey, T. *Z. Kristallogr.* 1966, **123**, 263
41 Nyquist, R.A. and Kagel, R.O. *Infrared Spectra of Inorganic Compounds*, Academic Press, London, 1971
42 Goullet, A., Camassel, J. and Pascual, J. in *Proceedings of the 11th International Conference on Raman Spectroscopy* (Eds. R.J.H. Clark and D.A. Long) Wiley, Chichester, 1988, p. 369
43 Richardson, J.W., Smith, J.V. and Han, S. *J. Chem. Soc., Faraday Trans.* 1990, **86**, 2341
44 de Man, A.J.M., Küppers, H. and van Santen, R.A., *J. Phys. Chem.* 1992, **96**, 2092
45 Ignat'ev, I.S., Lazarev, A.N. and Kolesova, V.A. *Inorg. Materials* 1976, 1024
46 Lazarev, A.N., Mirgorodskii, A.P. and Muldagaliev, K.K. *Inorg. Materials* 1976, 1032
47 Geidel, E., Birner, P. and Böhlig, H. *Z. Chem.* 1990, **30**, 141
48 Badger, R.M. *J. Chem. Phys.* 1934, **2**, 128
49 Badger, R.M. *J. Chem. Phys.* 1935, **3**, 710
50 O'Keefe, M., Domengés, B. and Gibbs, G.V. *J. Phys. Chem.* 1985, **89**, 2304
51 Dijkstra, C.E. *Ab-Initio Calculations of Structures and Properties of Molecules, Studies in Physical and Theoretical Chemistry*, Elsevier, Amsterdam, 1988
52 Pople, J.A., Schleger, H.B., Krishnan, R., Defrees, D.J., Binkley, J.S., Frisch, M.J. and Whiteside, R.A. *Int. J. Quantum Chem., Quantum Chem. Symp.* 1981, **15**, 269
53 Goullet, A., Camassel, J., Montaner, A., Pascual, J., Jumas, J.C. and Philippot, E. *Phys. Scr.* 1988, **37**, 395
54 Uytterhoeven, L., Mortier, W.J. and Geerlings, P. *J. Phys. Chem. Solids* 1989, **50**, 479
55 Dowty, E. *Phys. Chem. Minerals* 1987, **14**, 122
56 Miller, T.M. and Bederson, B. *Adv. At. Mol. Phys.* 1977, **13**, 1
57 Woodward, L.A. and Long, D.A. *Trans. Faraday Soc.* 1949, **45**, 1131
58 Allred, A.L. *J. Inorgan. Nucl. Chem.* 1961, **17**, 215
59 Blackwell, C.S. and Patton, R.L. *J. Phys. Chem.* 1984, **88**, 6135
60 Müller, D., Jahn, E., Fahlke, B., Ladwig, G. and Haubenreisser, U. *Zeolites* 1985, **5**, 53
61 Blackwell, C.S. and Patton, R.L. *J. Phys. Chem.* 1988, **92**, 3965